



## Johannes Spendier

## Analysis and Extension of the Knife-Edge Method

#### **BACHELOR THESIS**

to achieve the university degree of Bachelor of Science Bachelor's degree programme: Physics

submitted to

**Graz University of Technology** 

#### **Supervisor**

 ${\it Marcus~Ossiander,~Ass.Prof.~Dr.rer.nat.~B.Sc.~M.Sc.}$   ${\it Institute~for~Experimental~Physics}$ 

## Abstract

This work develops measurement software and protocols aimed at characterizing focused EUV light using a knife-edge method. For ease of development, the work was performed using visible light, which is easier to handle and (in contrast to EUV light) propagates in air. A CMOS camera sensor can be used to measure the intensity drop-off when moving the knife-edge into the beam. Using a laser in the visible range brings another advantage: the focus can also be measured directly with the CMOS camera sensor and then compared to the result of the knife-edge method, solidifying the results.

Classically, the knife-edge method performs a one-dimensional scan and requires assuming a spatial profile (usually a Gaussian) during data analysis. This is also done in this work to determine the beam diameter and the longitudinal position of the focus.

However, the beam shape can also be characterized using a second knife perpendicular to the first one, forming an L-shape. Cutting the beam in a pixel-like fashion by mounting the knifes on two perpendicular translation stages allows us to measure complete two-dimensional beam profiles without making assumptions about the profile beforehand. This makes the method more powerful for determining the shape of a laser beam and can reveal lens errors such as astigmatism and aberration.

Additionally, higher-order Laguerre-Gaussian modes are investigated by simulating the developed one- and two-dimensional techniques.

The developed methods and protocols were then used to measure 50-nm wavelength light focused by a toroidal mirror. It is planned for the future to use the technique to characterize high numerical aperture metalenses [1]. These metasurfaces focus EUV beams to below  $1\,\mu\mathrm{m}$  while not totally absorbing them. However, few optics exist that could image the produced foci, which predestines the knife-edge method to assess their performance.

## Contents

| 1             | Focused Laser Pulses  | 4                       |
|---------------|---|-------------------------|
| 2             | One-Dimensional Knife-Edge Measurements  2.1 Experimental Setup   | 5<br>7<br>8<br>11<br>12 |
| 3             | Two-Dimensional Knife-Edge Measurement  3.1 Measurement Protocol  | 14<br>14<br>15          |
| 4             | Higher-Order Mode Characterization (Simulation) 4.1 Mathematical Description of Higher-Order Laguerre-Gaussian Modes 4.2 Simulation Results of Higher-Order Laguerre-Gaussian Modes | 16<br>16<br>17          |
| 5             | Implementation in the EUV Beamline  5.1 General Experimental Setup for the EUV Beamline  5.2 Using the One-Dimensional Knife-Edge Method to Characterize the EUV Beam               | 21<br>21<br>21<br>21    |
| 6             | Conclusion  | 23                      |
| Li            | iterature   | 24                      |
| $\mathbf{Li}$ | ist of Figures  | 26                      |
| $\mathbf{A}$  | Measurement Software  | 27                      |

## Introduction

The knife-edge method has been used since before the invention of the laser to analyze the spatial beam profile of light [2]. Nowadays, high-resolution cameras, combined with imaging systems with high numerical aperture, often offer a more efficient way to analyze beam profiles. However, their effectiveness diminishes for beams focused below their resolution limit or when suitable imaging optics are unavailable for certain wavelengths. The knife-edge method offers an elegant solution to those challenges. In this approach, a sharp edge is moved into the laser beam step by step, and the corresponding intensity drop-off of the transmitted light is measured. This drop-off reveals the beam width at the current longitudinal position of the knife. Since the parameter of interest is the transmitted intensity, the resolution is determined not by the pixel density of a camera sensor, but solely by the precision of the translation stage used to move the knife [3].

Expanding this technique with a second, perpendicular knife allows for two-dimensional beam profiling, producing results comparable to those of a high-resolution camera.

Thus, the knife-edge method can characterize the width and even the entire twodimensional profile of light beams with high fidelity and without relying on imaging optics. This capability makes it particularly well-suited for characterizing EUV beams focused by metasurfaces, where cameras with resolutions around  $6\,\mu\rm m$  are insufficient for adequate focus imaging and suitable imaging optics are currently unavailable.

#### 1 Focused Laser Pulses

Often, the electric field E(x, y, z) emitted by a laser is considered to possess a Gaussian spatial beam profile. This assumption is made for several reasons, e.g., accurately describing the dominant mode a laser emits, ease of differentiability, symmetry, and the preservation of shape under Fourier transform. Most importantly, a Gaussian solves the paraxial wave equation 1.1. This equation assumes a profile along the x and y direction, that varies slowly compared to the propagation direction z [4]:

$$\frac{\partial E(x,y,z)}{\partial z} = -\frac{i}{2k} \Delta_t E(x,y,z) \tag{1.1}$$

Here,  $\Delta_t$  is the transversal Laplace operator, and k is the wavenumber. The intensity is then also Gaussian-distributed and connected to the electric field by

$$|E(x,y,z)|^2 \propto I(x,y,z) = I_0 \cdot \exp\left[-\frac{2(x-x_0)^2 + 2(y-y_0)^2}{w(z)^2}\right]$$
 (1.2)

In this case,  $x_0$  and  $y_0$  represent the positions where the intensity reaches its maximum. x and y correspond to the position we are interested in, and w(z) is the beam radius at position z along the optical axis. Furthermore, w also corresponds to the standard deviation  $\sigma$  of a Gaussian in the way  $w = \sqrt{2}\sigma$ . A detailed derivation of that can be found in [4].

A convex lens can focus such a Gaussian laser beam. The beam diameter decreases to a minimum in the focal plane of the lens and then starts growing again, as shown in Fig. 1.1. The beam radius w(z) changes as a function of the coordinate z according to

$$w(z) = w_0 \sqrt{1 + \left(\frac{z}{z_R}\right)^2} \tag{1.3}$$

Here,  $w_0$  is the beam radius at the position with the smallest beam waist along the z-axis and  $z_R$  corresponds to the so-called Rayleigh range, which is the distance at which the beam waist has increased to  $\sqrt{2}w_0$ .  $z_R$  is not a constant but a function of the wavelength  $\lambda$  of the incoming beam [2]:

$$z_R = \frac{\pi w_0^2}{\lambda} \tag{1.4}$$

I.e., the smaller the wavelength, the longer the Rayleigh range. Fig. 1.1 illustrates the change of the beam waist upon propagation.

The radial coordinate  $\rho^2 = x^2 + y^2$ , with the transverse coordinates in the plane of the beam x and y, is useful for treating beams with circular symmetry (e.g., Gaussian beams). The beam waist at each point along the optical axis, shown in Fig. 1.1, is defined as the location where the beam intensity drops to  $1/e^2$  of its maximum value in that plane. This typical convention corresponds to two standard deviations  $\sigma$  away from the center of a Gaussian beam [2]:

$$I(2\sigma) = I_0 \exp\left(-\frac{2w^2}{w^2}\right) = I_0 \cdot \exp\left(-\frac{(2\sigma)^2}{2\sigma^2}\right) = I_0 \exp\left[-2\right] = \frac{I_0}{e^2}$$
 (1.5)

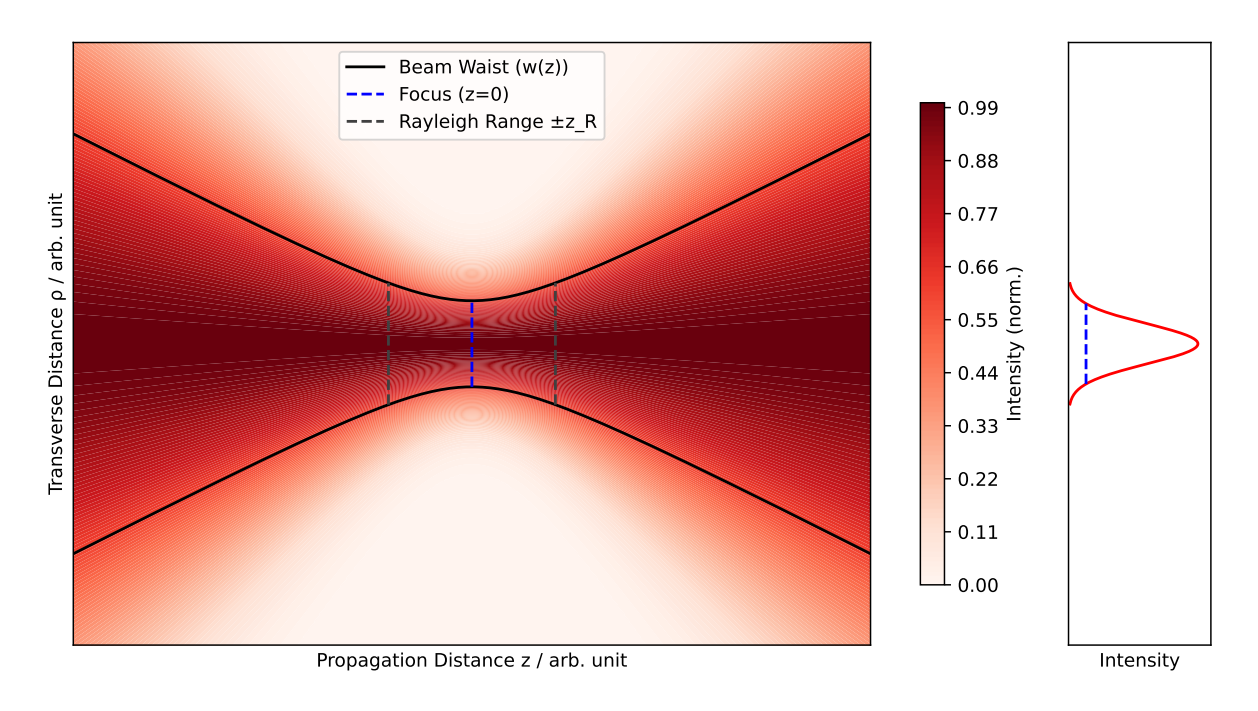


Figure 1.1: Left panel: beam waist evolution of a focused Gaussian laser beam. The color map represents its intensity distribution. The dashed gray line indicates the Rayleigh range  $z_R$ . Right panel: intensity distribution of the Gaussian beam profile in the focal plane. The blue dashed line indicates where the beam width is measured according to common convention [2].

## 2 One-Dimensional Knife-Edge Measurements

Now we are going to examine what happens when we block part of the light beam with a knife-edge. Fig. 2.1 illustrates the one-dimensional knife-edge principle. A laser beam

is coming from the left and is focused by a lens. Part of the beam waist is blocked as the knife moves into the beam [5]. Depending on the position of the knife along the optical axis z, the camera will show the transmitted part of the beam either on the bottom, if the knife is in front of the focus or on top, if the knife is behind the focus. This can be useful in experimental setups to determine the current position of the knife along the optical axis.

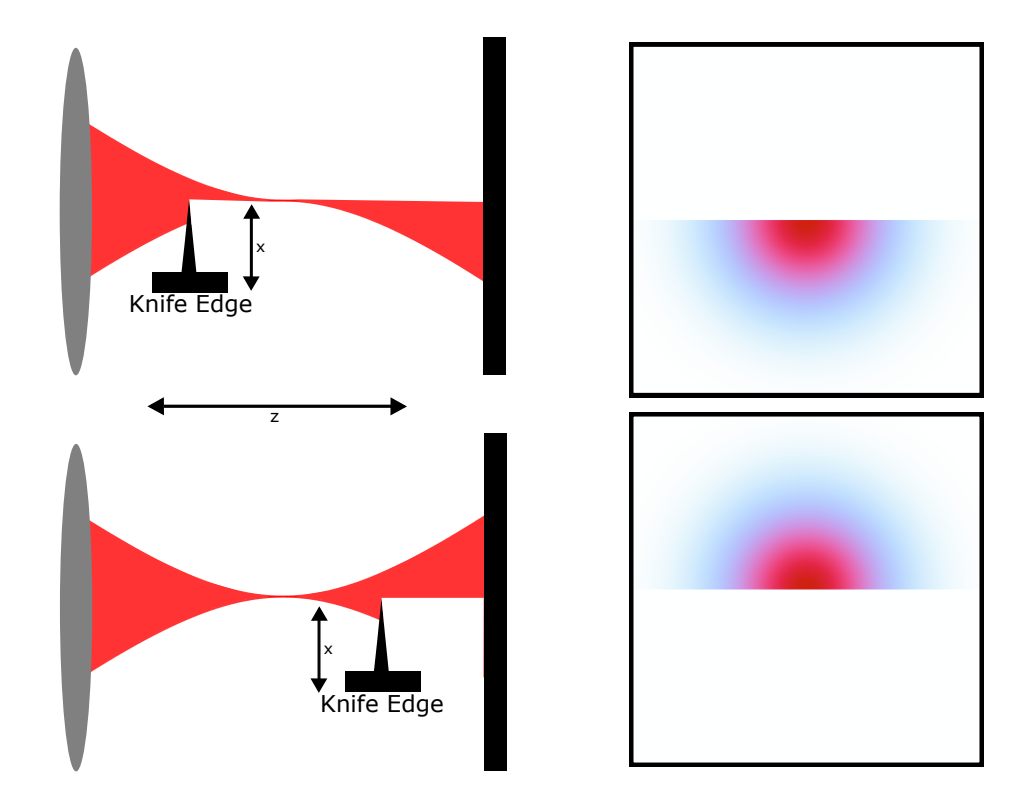


Figure 2.1: Illustration of the knife-edge blocking part of the laser beam. The black bars indicate where the camera sensor sits. If the knife is placed in front of the focus, the camera will show the knife-edge at the top. If the knife is placed after the focus, the camera shows the knife-edge at the bottom. The two panels on the right show what the camera would capture when the knife is positioned in front of or behind the focal plane, respectively.

If we assume a Gaussian intensity distribution I(x, y) for the Laser, we can split it into two independent distributions I(x) and I(y). This also applies to our measurement value, the transmitted power P(x, y), since we can integrate the intensity distributions I(x) and I(y) separately to get  $P(x) \cdot P(y)$ . The position of the knife is denoted as x. Since we measure with a single knife along the x-axis, the second dimension along y automatically gets integrated from minus to plus infinity and therefore just yields an additional constant  $P_y$  [2]. c is a constant that depends on the intensity factor  $I_0$  and w

as well as the factor  $P_y$ :

$$P(x,y) = P(x) \cdot [P(y)]_{-\infty}^{\infty}$$

$$= \int_{x}^{\infty} I(x) dx \cdot P_{y}$$

$$= \int_{x}^{\infty} I_{0} \cdot \exp\left[-\frac{2(x-x_{0})^{2}}{w^{2}}\right] dx \cdot P_{y}$$

$$= c \cdot \left(1 - \operatorname{erf}\left(\frac{\sqrt{2}(x-x_{0})}{w}\right)\right)$$
(2.1)

Eq. 2.1 illustrates how the experiment should be performed. Data for the function P(x) can be gathered by positioning the knife at different positions x. The total transmitted power should be measured, which corresponds to the integration over x in eq. 2.1. These data points should describe an error function that drops off as more of the beam is blocked by the knife [6].

To then derive the intensity distribution I(x) from the measured data, one has to differentiate with respect to x. This yields a data series that can be fitted with a Gaussian intensity distribution, from which the waist size w can determined according to eq. 1.5. Data can be gathered at several positions along z to find the position where the beam diameter is smallest, and therefore closest to the focus. Since the beam width gets smaller at the focus, the error function changes more quickly. This means it gets steeper the closer the knife-edge gets to the focus. An illustration of this circumstance can be seen in Fig. 2.2. The part blocked by the knife-edge is indicated in the graph as a gray area.

## 2.1 Experimental Setup

This section describes the data we gathered from one-dimensional knife-edge experiments. A minimum beam waist will be calculated from the knife-edge data, as well as from the camera image directly.

Fig. 2.3 shows the experimental setup. We use a laser beam from a laser pointer with a wavelength of  $520\,\mathrm{nm}$  and a power of  $1\,\mathrm{mW}$ . An iris placed just after the exit of the laser cuts off disturbing parts. A convex lens L1 with a focal length of  $60\,\mathrm{mm}$  focuses the beam. A second lens L2 with  $f=40\,\mathrm{mm}$  after the focus images the focal plane on a CMOS camera (model: IDS uEye U3-3560XCP-M-NO). We use a Python script to visualize the camera data. Two optical components between lens L2 and the camera reduce the intensity to avoid camera saturation. First, a beam splitter splits off 99 % percent of the beam. Then, an ND2 filter further attenuates the transmitted beam.

We use a commercially available razor blade as a knife-edge. It is mounted on a nanopositioning stage that moves the blade up and down into the beam. This movement corresponds to the x-axis. The stage with the knife is then mounted to another nanopositioning stage that is oriented along the optical axis z. The stages can be moved with a Python package or the corresponding software by attoCUBE. The knife-edge is mounted close to the focus, as the range of the nanopositioning stage (30 mm) along the optical axis is limited. The approximate focus position of the laser can be found by using a white sheet of paper and observing where the laser beam is smallest. It is clear that the focus will be close to the focal length of the first focusing lens L1, since the incoming beam is

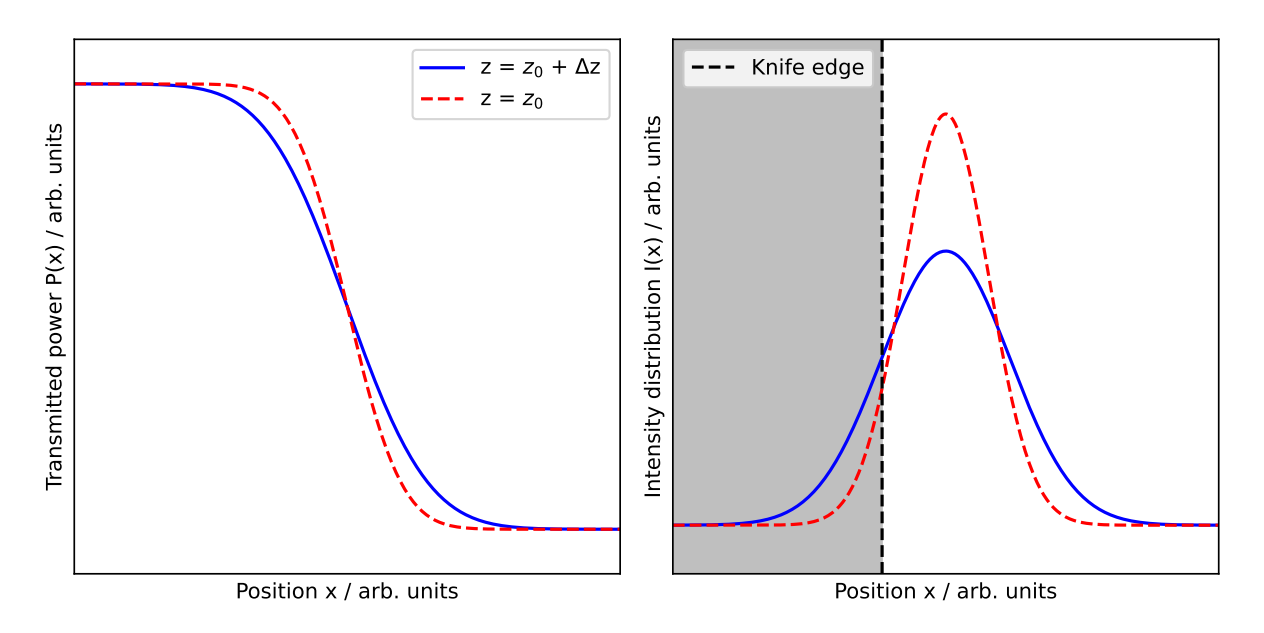


Figure 2.2: Illustration of the functions that describe the experiment.  $z_0$  is the position of the focal plane along the optical axis. The error functions on the left describes the drop-off in transmitted Power P(x) that happens when the knife-edge is moved into the beam. The right graphs show the derivatives of the left ones. They resemble the Gaussian intensity distribution of the beam. The red graphs are at the focal plane  $z_0$  and the blue graphs are  $\Delta z$  away from the focal plane. The knife-edge is indicated as the gray area, which cuts of the Gaussian intensity distribution.

more or less parallel. This can be of help in finding a reasonable mounting position for the knife-edge.

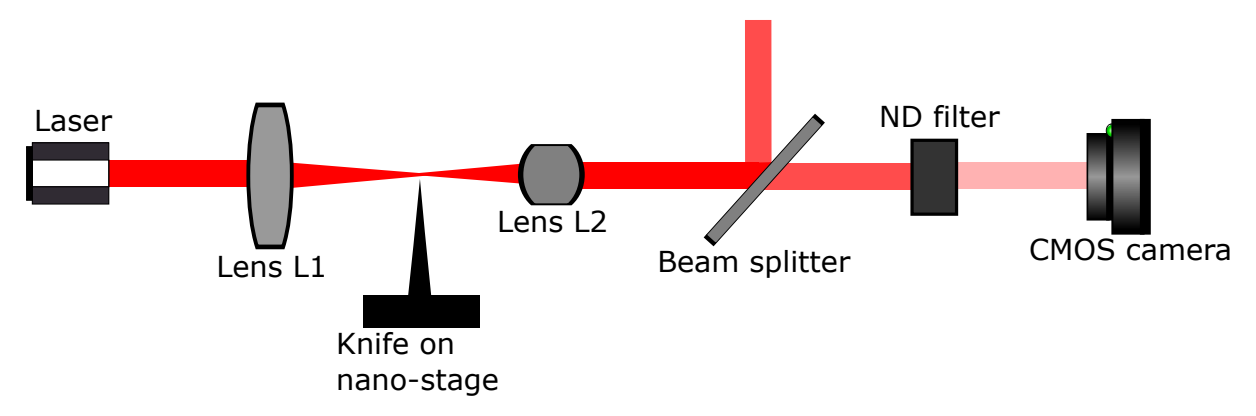


Figure 2.3: Illustration of the experimental setup. A 520-nm wavelength laser is focused by lens L1. The knife-edge is placed on nano-stages, that can move the knife perpendicular and parallel to the beam. A beam splitter and an ND filter are used to reduce the intensity hitting the CMOS camera.

#### 2.2 Measurement Protocol

The knife-edge is moved through the beam in increments of  $3 \mu m$ . Figure 2.4 shows some representative camera images capturing the beam as it is progressively cut off. Furthermore, interference patterns are visible in the images, which might influence the

measurement and will be discussed later. The knife is moved 40 times along the x-axis, corresponding to 40 data points. A window was defined around the beam in the camera image, from which we extract the integrated average intensity value to minimize noise. After we performed one measurement series at position z, the knife is moved out of the beam and shifted by  $250\,\mu\mathrm{m}$  along the optical axis z. At the new position z, we move the knife in 40 steps through the beam again. This procedure is repeated at eight positions along z. Four of those eight data sets can be seen in Fig. 2.5.

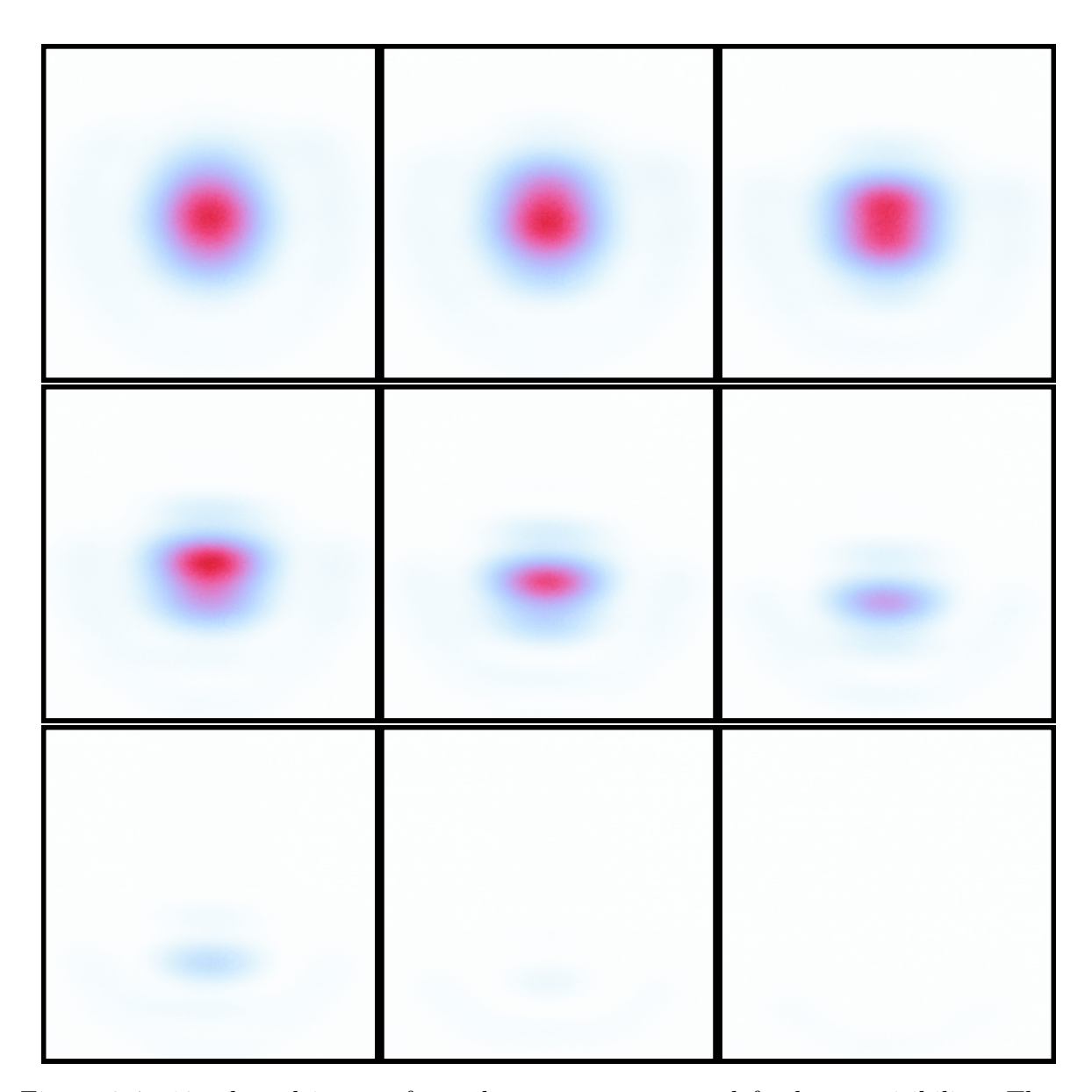


Figure 2.4: 12 selected images from the camera, processed for better visibility. These images are cropped to show only the beam. They demonstrate how the knife moves through the beam when it is close to the focus.

Fig. 2.5 shows that the data matches the fitted error function P(x). To obtain the derivative, the finite difference method was used. This numerical derivative was then fitted with the Gaussian intensity distribution I(x). The parameters from the plots

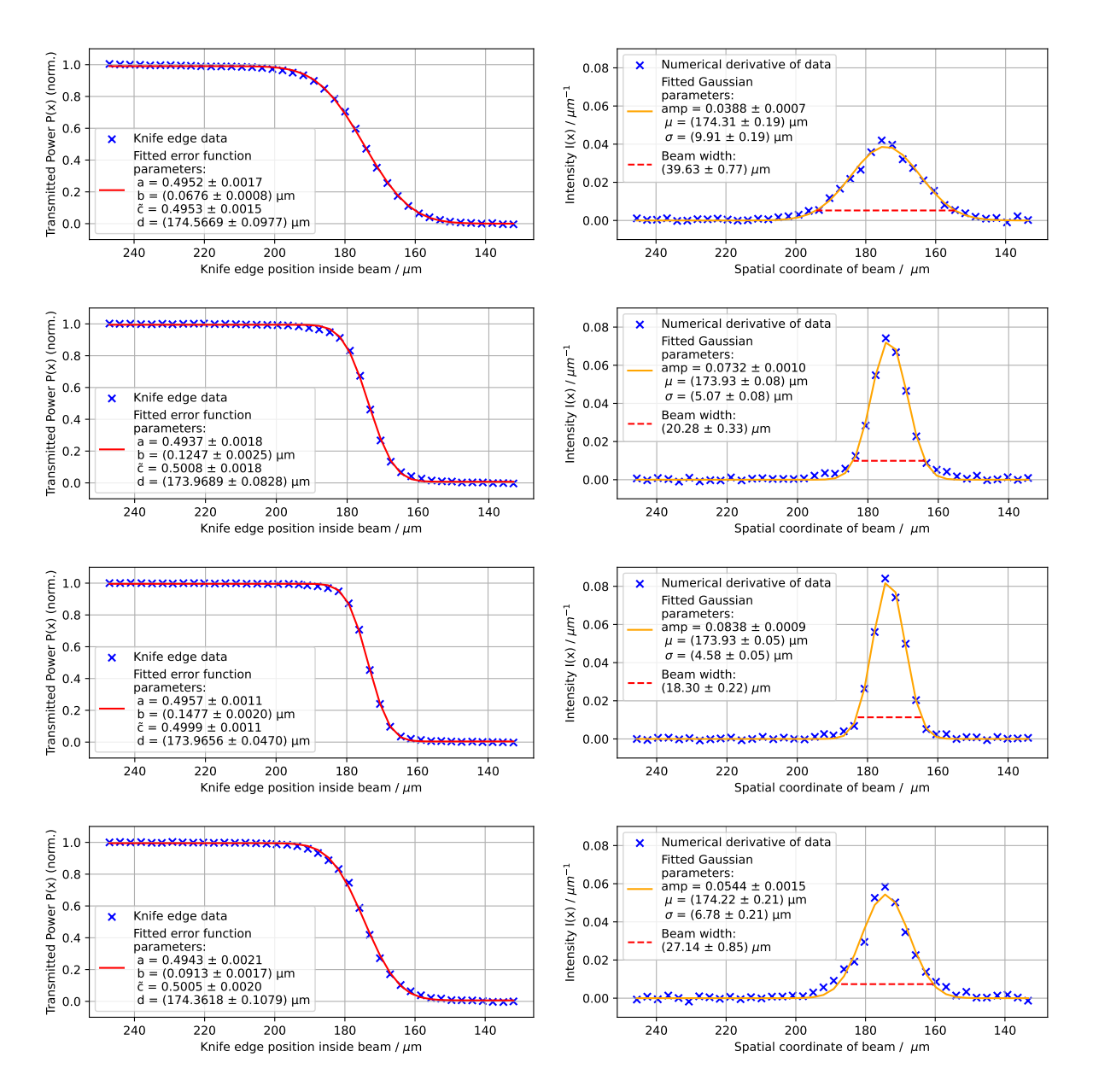


Figure 2.5: Experimental data and its numerical derivative. The experimental data is plotted on the left side (blue) and fitted with an error function (red). The numerical derivative of the data points (blue) can be seen on the right side. It is calculated via the finite difference method and then fitted with a Gaussian (orange). The position changes by  $50\,\mu\mathrm{m}$  along the optical axis for every row of graphs. The errors of the fitted parameters were calculated according to eq.2.2.

correspond to the following functions:

$$P(x) = a \cdot \operatorname{erf} (b \cdot (x - d)) + \tilde{c}$$
$$I(x) = \operatorname{amp} \cdot \exp \left(-\frac{(x - \mu)^2}{2 \cdot \sigma^2}\right)$$

The corresponding errors of the parameters error<sub>parameter,i</sub> are calculated via,

$$\operatorname{error}_{\operatorname{parameter,i}} = \sqrt{M_{\operatorname{covariance,ii}}}$$
 (2.2)

where M is the covariance matrix from the Python package scipy, which we used to fit the data. The diagonal elements ii of the matrix give the variance of the corresponding parameter and their square root is the standard deviation. The model of the package assumes a linear approximation near the optimum solution for the calculated parameters to get their variances. This means that close to the optimal solution, the model assumes that small changes in the parameters yield small changes in the model output [7]. We will use this method throughout the thesis when calculating fit errors.

Fig. 2.5 shows that the error functions first steepens up to a certain position along z and then flattens again. This gets even clearer when looking at the derivatives on the right side, since first the maximum increases and then decreases again. The beam width can be extracted from the Gaussian fits by measuring their width at  $1/e^2$  of the maximum, as suggested in eq. 1.5. The plot showing the smallest beam width already gives an estimate for the minimum. The smallest beam width in the plots is  $(18.3 \pm 0.3) \,\mu\text{m}$ . The beam waist w(z) is half the width:  $(9.15 \pm 0.15) \,\mu\text{m}$ . The focus therefore has to be at least that small or smaller because w(z), see eq. 1.3, is a convex function.

To determine the minimum beam waist more precisely, we fit the dataset of beam waists w(z) with eq. 1.3, which describes the beam waist of a focused Gaussian beam. From the fitted beam waist function in Fig. 2.6, we get a minimum beam radius of

$$w_{0,knife} = (7.6 \pm 1.4) \,\mu\text{m}$$

The minimum occurs at  $z = (4.36 \pm 0.04)$  mm. The position z along the optical axis is determined from the stage and therefore a relative value.

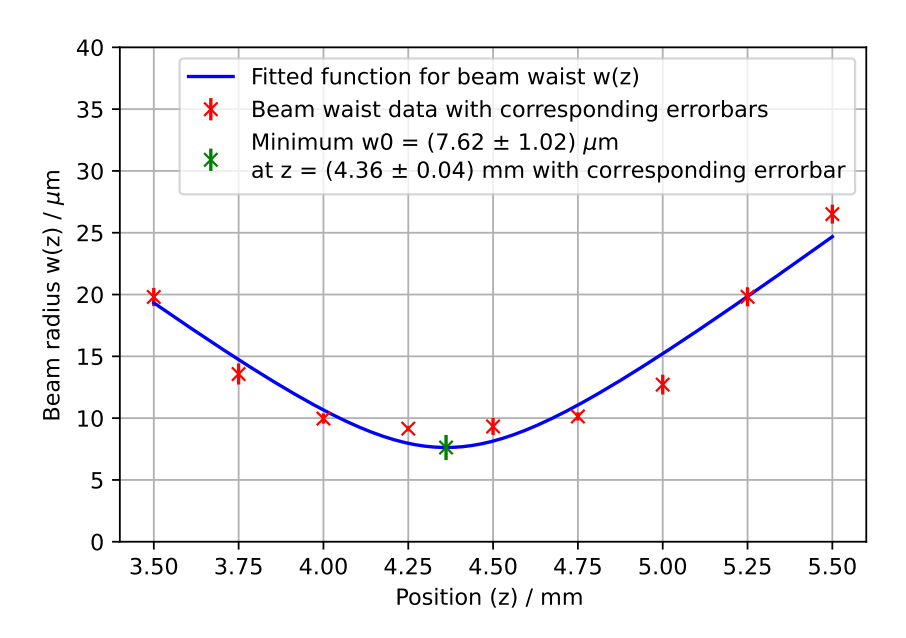


Figure 2.6: Fitted data for the beam waist w(z). The fit function is given by eq. 1.3. The data points are marked in red. The minimum of the fit is marked in green.

## 2.3 Comparison to the Imaged Focus

Since the camera and imaging system have a high enough resolution we can also measure the focus size directly when accounting for the magnification. The position of the camera is varied to determine the highest intensity, which corresponds to the position where lens L2 projects the focus. This position was found around  $(53.0\pm0.5)$  cm after lens L2, which corresponds to the image distance b. The distance between the knife-edge and the second lens (L2) was  $(3.3\pm0.2)$  cm, corresponding to the object distance g. Consequently the magnification M of the imaging system is [8]:

$$M = \frac{b}{q} = (16.0 \pm 1.2) \tag{2.3}$$

We used the derivative method for error propagation. It is done via a function in *Excel* [9], which calculates the difference quotient in an interval of  $\Delta x = x \cdot 10^{-8}$ . This error propagation method will be used for the rest of this thesis.

To compare the minimum beam waist obtained from the image in Fig. 2.7 with the result from the knife-edge method, we read the image into Python. The sum of the pixels along the vertical axis is taken. The resulting one-dimensional data series is then fitted with a Gaussian (Fig. 2.8a). From the fit, the beam waist can be determined according to eq. 1.5. This gives a beam waist of  $(46.49 \pm 0.14)$  px.

Since the radius is now given in pixels (px), we need to convert to micrometers ( $\mu$ m). The resolution of 1920x1080 px and the camera sensor dimensions of 5.76 mm  $\times$  3.6 mm yield a pixel size of 3  $\mu$ m. We convert the radius into micrometers by multiplying the waist in pixels by the pixel size and then dividing by the magnification factor:

$$w_{0,\text{img,vertical}} = (8.7 \pm 0.7) \,\mu\text{m}$$

We apply the same procedure to find the beam waist along the horizontal-axis (refer to Fig. 2.8b). The waist in pixels is  $(44.6 \pm 0.3)$  px. This gives a slightly different result:

$$w_{0,\text{img,horizontal}} = (8.3 \pm 0.7) \,\mu\text{m}$$

The results indicate that the beam is not circular, however, with only a slight deviation. This deviation could be attributed to astigmatism in one of the lenses. Additionally, the initial laser beam might not be circular.

Furthermore, the noise in Fig. 2.8a is larger than in Fig. 2.8b. Since the data analysis was identical in both cases, the difference in noise is attributed to the camera and how the intensity is evaluated by the sensor.

Over all, the results for the minium beam waist along the vertical axis  $w_{0,\text{img,vertical}}$  solidifies what we measured with the knife-edge method  $(w_{0,knife} = (7.6 \pm 1.4) \,\mu\text{m})$ , since the uncertainties overlap.

# 2.4 Analysis of the Beam's Central Cross Section and Notable Features in the Data

One can also examine a single pixel row through the center of the beam. The center was determined using the fits from Fig. 2.8a and Fig. 2.8b, where the peak of the Gaussian was assumed to represent the center. This analysis was performed for both the horizontal and vertical axes. The resulting data is then fitted with Gaussian distributions again, as shown in Fig. 2.9a and Fig. 2.9b. The waists obtained from these fits are:

$$w_{0,imq,horizontal,CUT} = (8.3 \pm 0.6) \,\mu\mathrm{m}$$

$$w_{0,img,vertical,CUT} = (8.1 \pm 0.6) \,\mu\mathrm{m}$$

Looking at Fig. 2.8b and also Figs. 2.9a and 2.9b provides an interesting perspective for later simulations. A knife-edge measurement might be able to detect interference patterns. The small bumps next to the Gaussian fit in both figures seem to align well with the positions of the interference patterns that can be seen in Fig. 2.7. These interference rings might be attributable to the aperture placed in the beam.

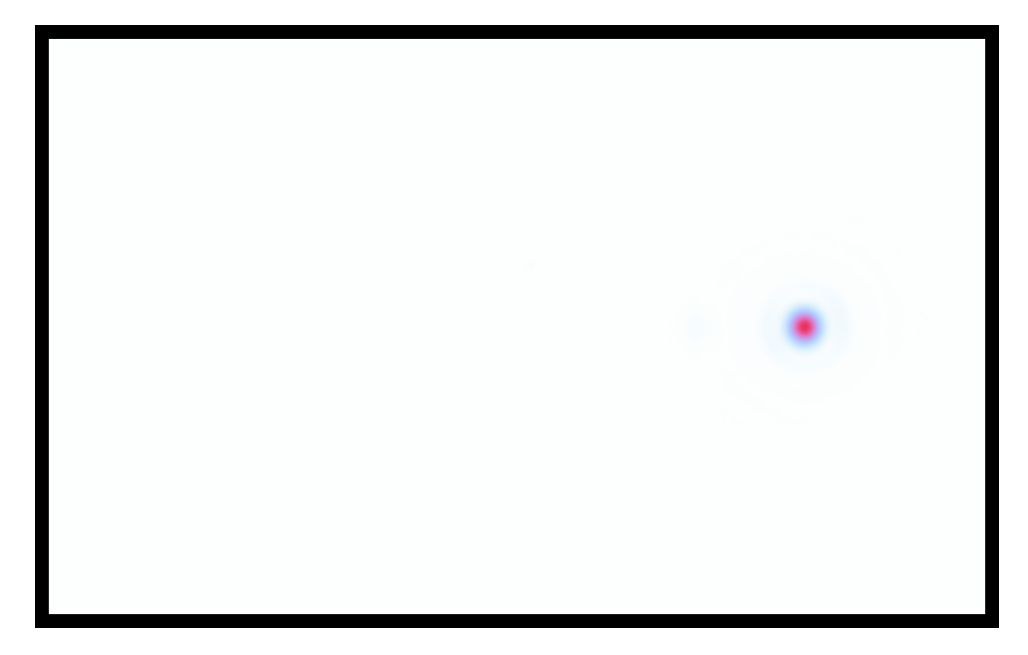
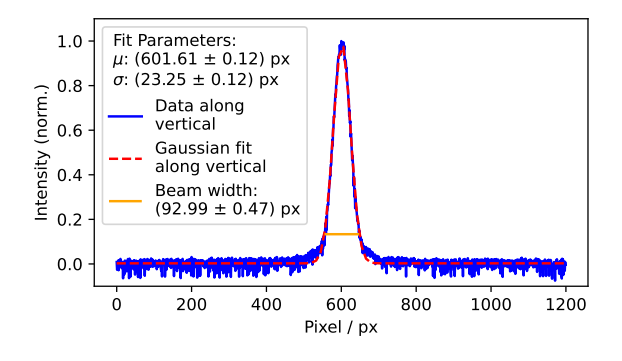
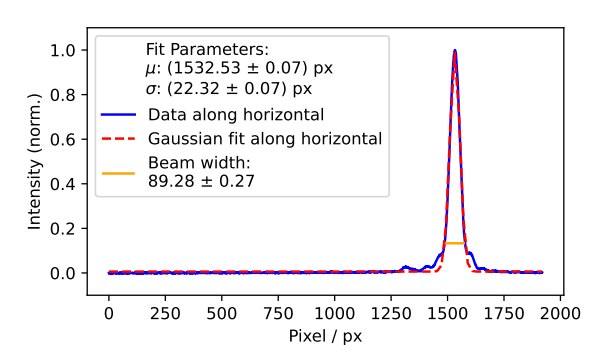


Figure 2.7: CMOS image used to determine the beam waist in the focal plane.

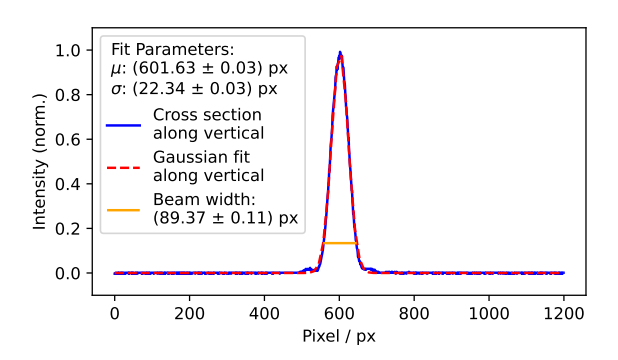


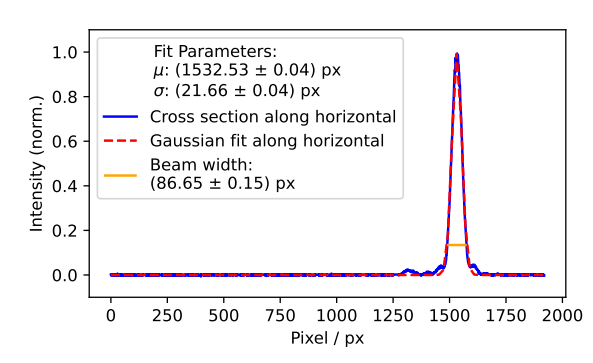


(a) Data with Gaussian fit from image 2.7. The data along the horizontal axis was summed up. Remaining vertical data (blue) was fitted with a Gaussian distribution (red). Fit parameters with according errors are shown in the plot.  $\sigma$  is the standard deviation,  $\mu$  is the mean. The beam width is indicated in orange.

(b) Data with Gaussian fit from image 2.7. The data along the vertical axis was summed up. Remaining horizontal data (blue) was fitted with a Gaussian distribution (red). Fit parameters with according errors are shown in the plot.  $\sigma$  is the standard deviation,  $\mu$  is the mean. The beam width is indicated in orange.

Figure 2.8: Camera data along the vertical (left panel) and horizontal (right panel) direction. The remaining dimension was summed.





the beam from Fig. 2.7 is plotted in blue. This row of data is fitted with a Gaussian (red).  $\sigma$ is the standard deviation,  $\mu$  is the mean. The beam width is indicated in orange.

(a) One vertical pixel row through the center of (b) One horizontal pixel row through the center of the beam from Fig. 2.7 is plotted in blue. This row of data is fitted with a Gaussian (red).  $\sigma$  is the standard deviation,  $\mu$  is the mean. The beam width is indicated in orange.

Figure 2.9: Vertical (left panel) and horizontal (right panel) cross sections through the center of the beam.

#### Two-Dimensional Knife-Edge Measurement 3

One can also think of a method to measure the intensity distribution I(x,y) in two dimensions. For that we need to gather data points P(x,y), with x and y being the coordinate axes perpendicular to the optical axis. Eq. 2.1 then has to be adjusted to include the other dimension [2].

$$P(x,y) = \int_{y}^{\infty} \int_{x}^{\infty} I(x,y) \, dx \, dy \tag{3.1}$$

I(x,y) is the intensity at point x and y. The experimental setup from Fig. 2.3 has to be changed accordingly. A second knife is placed perpendicular to the first one to form an L-shape. This allows measuring P(x,y) at position (x,y). If the knife is at position (x,y), this corresponds to an integration of the intensity starting from those values up to infinity in eq. 3.1. So the two-dimensional intensity distribution I(x,y) within the beam can be calculated by taking the derivative along both directions:

$$I(x,y) = \frac{d}{dx}\frac{d}{dy}P(x,y) = \frac{d}{dx}\frac{d}{dy}\int_{y}^{\infty}\int_{x}^{\infty}I(x,y)\,dx\,dy$$
 (3.2)

Since we measure a full two-dimensional intensity distribution according to this method, no assumptions about the distribution have to be made in contrast to the one-dimensional method. The one-dimensional method already integrates over one of the axes during the measurements. This loss of information, required us to make to make the assumption that we can split P(x,y) into two independents functions  $P(x) \cdot P(y)$ , see eq. 2.1.

#### Measurement Protocol 3.1

To gather data points for the function P(x,y), the knife follows a specific movement pattern. First, it moves one step of  $5\,\mu\mathrm{m}$  along the x-axis. Then, it takes 20 steps of 5  $\mu$ m along the y-axis. After reaching the final y-position, it returns to the starting position along the y-axis. The knife then moves one step along the x-axis and repeats the stepping process along y for another 20 steps. This whole process is repeated at 12 different positions along the optical axis z with a step size of  $250\,\mu\mathrm{m}$ . With  $20\mathrm{x}20$  steps in the optical plane, we gather 400 data points at every position along z. For further explanation on how the data is gathered, refer to Sec. 2.2. Fig. 3.1 is an exemplary image of what the camera sees when the L-shaped knife moves through the beam in this pixel-like measurement.

To get the two-dimensional intensity profile, one can use a numerical differentiation method in compliance with eq. 3.2. The data points of P(x, y) first get numerically differentiated along x and then along y. This yields a two-dimensional matrix that describes the intensity distribution.

#### 3.2 Results

Fig. 3.2 shows the data matrices; the color code describes the intensity. The images depict what we expect: With changing position along z, the beam diameter gets smaller and smaller and then larger again. Therefore, the focus has to be around the position that corresponds to the bottom-left image in Fig. 3.2. This image depicts the result with the smallest beam size and the highest maximum intensity we measured. With smaller steps in the x and y directions, the resolution would improve. However, increasing the number of steps along x and y yields quadratically more measurement points, which elongates the acquisition time enormously. The maximum possible resolution is around 50 nm. This is due to the minimum step size of the stages. A step size of 50 nm would yield a resolution that is about 100 times better than what we used. For usage in more tightly focused beams, such as EUV beams focused by metalenses [1], this higher resolution can become important.

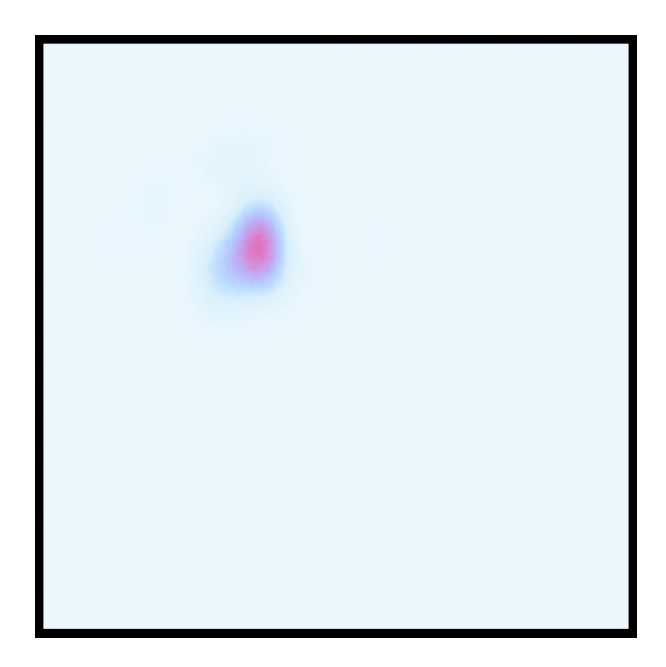


Figure 3.1: Image by the CMOS camera of the beam while the L-shaped knife moves through it.

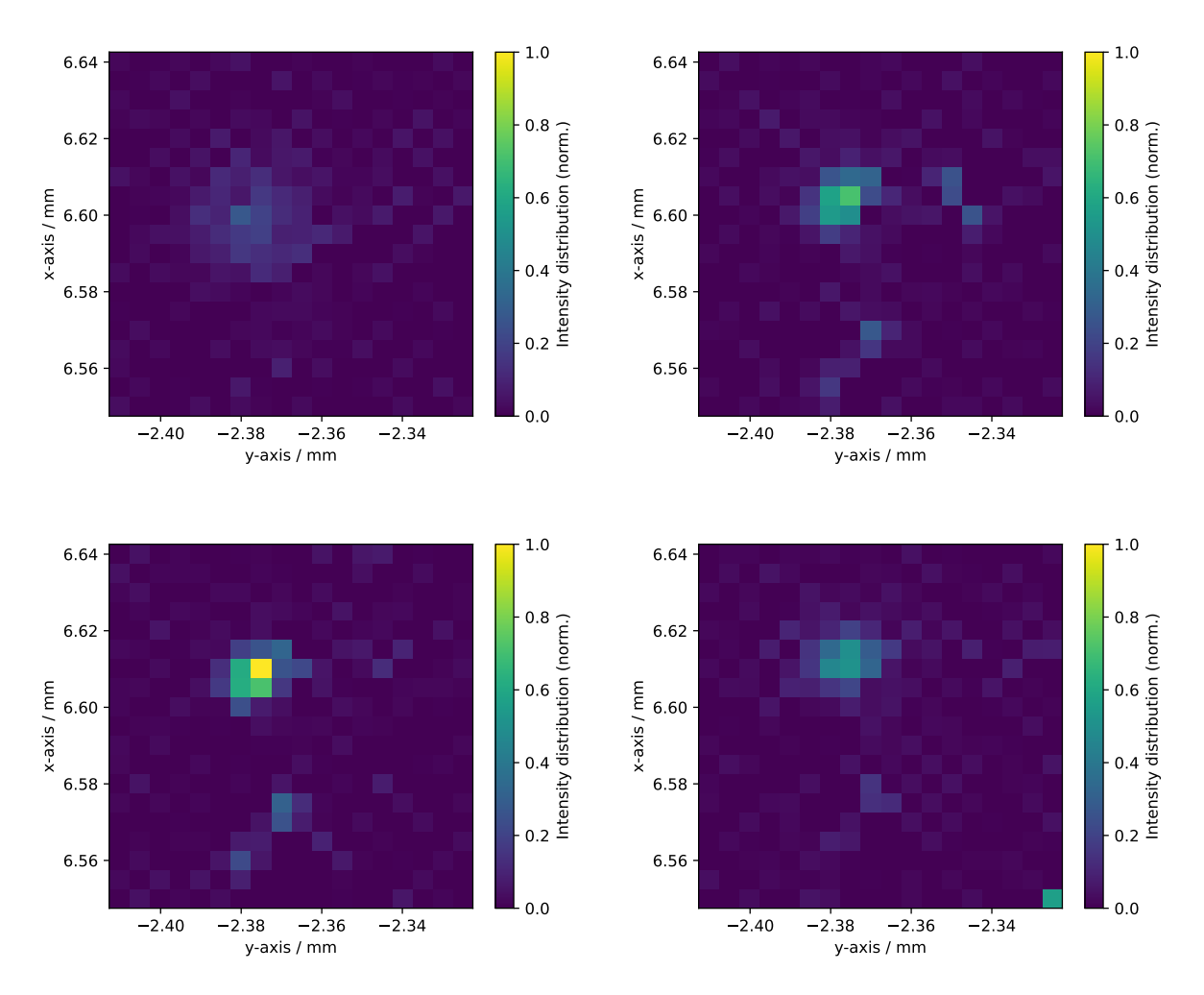


Figure 3.2: Experimentally determined intensity distributions. The upper two images are about 1 and 0.5 mm before the focus. The intensity is scaled from 0 to 1. Intensity of 1 corresponds to the maximum in the bottom-left image, which is closest to the focal plane. The bottom right image is about 0.5 mm after the focus.

## 4 Higher-Order Mode Characterization (Simulation)

Up to this point, the laser beam was assumed to be a zero-order Gaussian mode. However, one can also consider higher-order modes. We limit ourselves here to higher-order Laguerre-Gaussian modes, since those reproduce the observed ring shapes, that can be seen in Fig. 2.7. We will simulate what one- and two-dimensional knife-edge measurements could gather by using them on these higher-order beams. We will also consider how noise affects the data.

### 4.1 Mathematical Description of Higher-Order Laguerre-Gaussian Modes

Laguerre-Gaussian modes also solve the paraxial wave equation from Sec. 1, however in cylindrical coordinates. Their intensity distributions have the form [4]:

$$I_{LG}(\rho, l, p) \propto \operatorname{const}(l, p) \cdot \left(\frac{2\rho^2}{w(z)^2}\right)^{|l|} \cdot |L_p^{|l|} \left(\frac{2\rho^2}{w(z)^2}\right)|^2 \cdot \exp\left(-\frac{2\rho^2}{w(z)^2}\right)$$
(4.1)

Here,  $L_p^{|l|}$  are the Laguerre polynomials and l,p are integers describing the order of the polynomial.  $\rho$  is the radius  $\sqrt{x^2 + y^2}$ , and w(z) is the beam waist function at position z along the optical axis. For brevity, the prefactor is written as a constant.

# 4.2 Simulation Results of Higher-Order Laguerre-Gaussian Modes

The simulation works as follows: We create a fine grid along x and y. We then plug these values into eq. 4.1 using  $\rho^2 = x^2 + y^2$ . This gives us an intensity distribution  $I_{\text{LG,ref}}(r,l,p)$ , which we use as a reference to know how the actual beam looks. We also generate another grid with fewer data points. The size of the pixels in the coarse grid corresponds to the step size of the knife. For this grid, we also calculate the intensity distribution. We then add a Matrix  $M_{\text{noise}}$  of Gaussian noise in the following way:

$$M_{\text{noise}} = \text{noise level} \cdot G_{\text{Gauss noise}}$$
  

$$\Rightarrow I_{\text{LG}}(\rho, l, p) + M_{\text{noise}} = I_{\text{LG,noisy}}(\rho, l, p)$$
(4.2)

The noise matrix,  $M_{\text{noise}}$ , is the product of the specified noise level (ranging from 0 to 1) and a Gaussian-distributed matrix  $G_{\text{Gauss noise}}$ , with mean 0 and standard deviation 1. A noise level of 1 indicates that the values in  $M_{\text{noise}}$  have magnitudes comparable to the intensity matrix  $I_{\text{LG}}(r,l,p)$ , which was also scaled between 0 and 1. The resulting matrix  $I_{\text{LG,noisy}}$  is then integrated numerically to get a new matrix  $P(x,y)_{\text{noisy}}$ , which corresponds to the data one would expect from a two-dimensional knife-edge measurement. We then perform the same procedure as in the actual experiment, taking the numerical derivative of the matrix along the horizontal axis, and then along the vertical axis. This gives an approximate result for the intensity distribution one could expect from an actual experiment. Furthermore, we also simulate what one would expect for a one-dimensional knife-edge measurement along the horizontal and the vertical axis. For that, we sum over one axis of our two-dimensional distribution and plot the resulting data series as a function of the remaining spatial coordinate.

#### Simulation of the $I_{LG}(\rho, l = 2, p = 0)$ -Mode

First, we simulate the  $I_{LG}(\rho, l=2, p=0)$ -mode, to see if ring shapes can be resolved. The result is shown in Fig. 4.1. The donut shape of the Laguerre-Gaussian beam is reproduced by the two-dimensional knife-edge measurement, even with an added noise level of 0.15. The step size of the knife is  $0.1_0$  (unit is in numbers of the minimum beam waist  $w_0$ ). This step size is practical, as the stage resolution of 50 nm would still yield 10 measurement points inside a beam with a waist of 500 nm. If the shape of the beam is cylindrically symmetric, the colormap plot in Fig. 4.1d does not provide much extra information compared to the one-dimensional simulations in Figs. 4.1e and 4.1f. The two maxima in the plots also indicate the donut shape of the beam. It becomes clear that the advantage of the two-dimensional measurement lies in the fact that it could reproduce intensity distributions that are not symmetric.

#### Simulation of the $I_{LG}(\rho, l = 0, p = 2)$ -Mode

The result for the  $I_{LG}(\rho, l = 0, p = 2)$ -mode is shown in Fig. 4.2. The two-dimensional simulation of the knife-edge measurement in Fig. 4.2d gives the expected result. The step

size is  $0.1 \,\mathrm{w_0}$ . The third ring, refer to Fig. 4.2a, is no longer visible in the two-dimensional knife-edge simulation in Fig. 4.2d due to its low intensity and a noise level of 0.08. Despite this, looking at the Figures for the one-dimensional method, 4.2e and 4.2f, we can still suspect a bump in the outer region, which might correspond to the third ring.

The two-dimensional distribution provides the beam profile without knowing anything about its symmetry or shape, but some details may be obscured by noise if the intensity or the signal to noise ratio is too low in certain areas. It is reasonable that noise has a greater impact on the quality of the data in the two-dimensional method. This is because the one-dimensional method effectively integrates over one dimension, which helps smooth the data and enhance details.

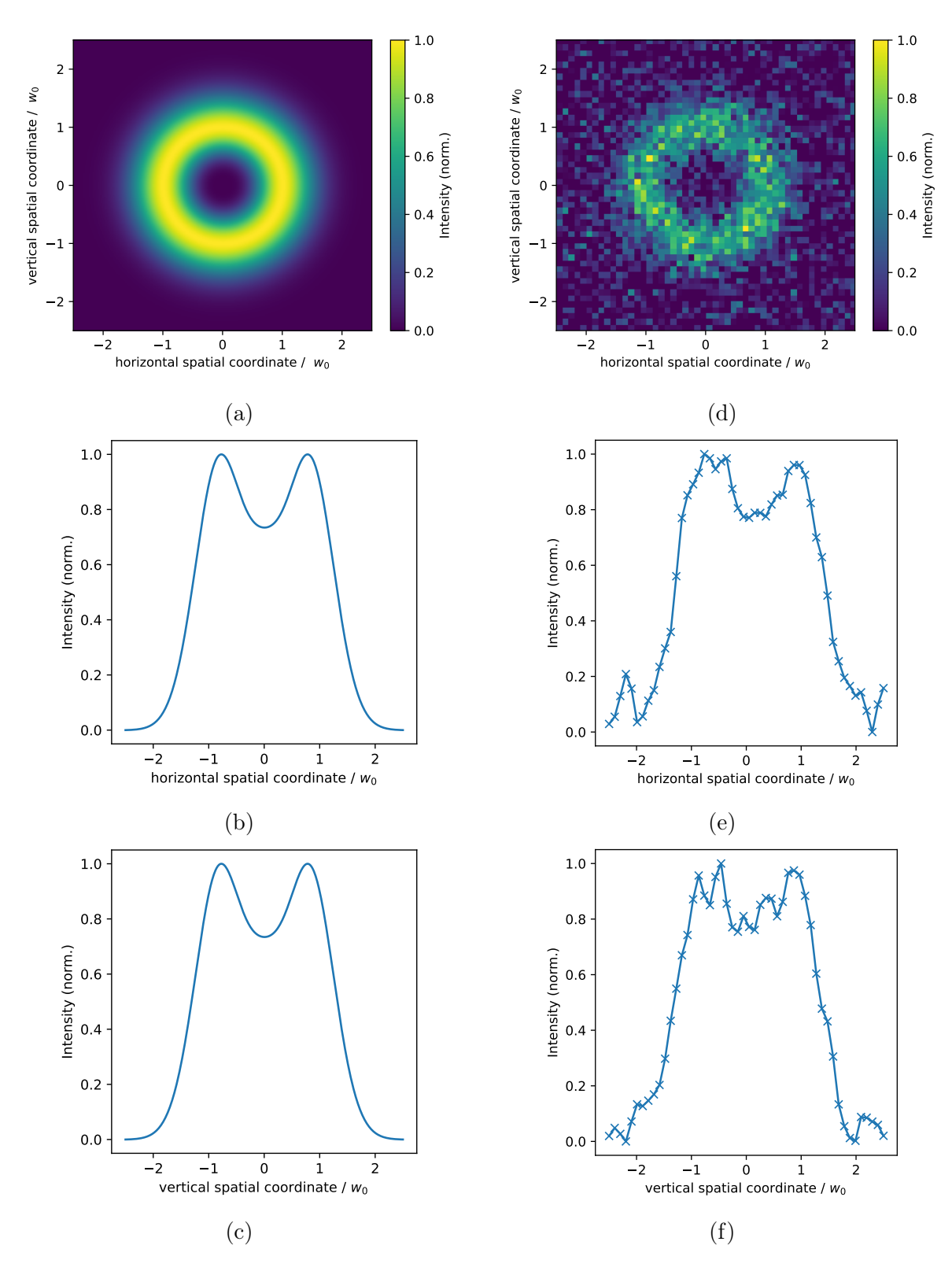


Figure 4.1: The left column of images shows the beam profiles from the simulation of the  $I_{LG}(\rho, l=2, p=0)$ -mode. The images in the right column show the results of the simulated knife-edge measurements with added noise level of 0.15. The "x" markers indicate the positions of the knife. The graphs in the second and third row show the same data as in the first row, however summed along one axis. They correspond to one-dimensional beam profiles.

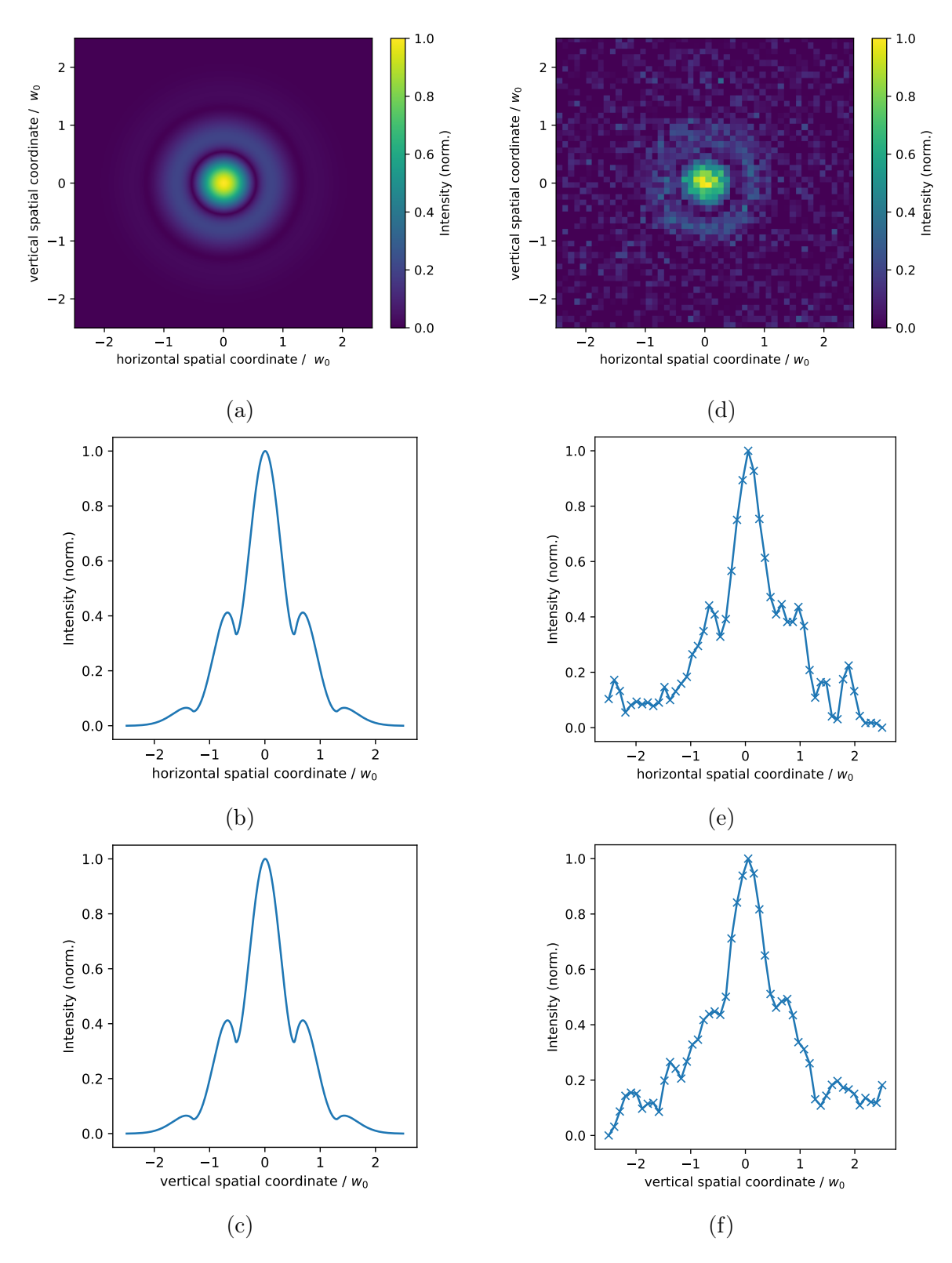


Figure 4.2: The left column of images shows the beam profiles from the simulation of the  $I_{\rm LG}(\rho,l=0,p=2)$ -mode. The images in the right column show the results of the simulated knife-edge measurements with added noise level of 0.08. The "x" markers indicate the positions of the knife. The graphs in the second and third row show the same data as in the first row, however summed along one axis. They correspond to one-dimensional beam profiles.

## 5 Implementation in the EUV Beamline

### 5.1 General Experimental Setup for the EUV Beamline

The complete setup is in vacuum, as the EUV beam is absorbed by air. An infrared laser is used to produce EUV light through high-harmonic generation (HHG) in a target. For more information, see, e.g., [10]. A toroidal mirror focuses the beam. The mirror is placed at a distance of two focal lengths  $2f = 72 \,\mathrm{cm}$  from the source. The knife-edge is then placed at a distance of 2f away from the focusing mirror. This setup is well-suited when considering the imaging equation, which for a 2f - 2f setup yields [8]:

$$\frac{1}{f} = \frac{1}{2f} + \frac{1}{q} \Rightarrow g = 2f \tag{5.1}$$

Thus, the 2f-2f setup results in a symmetric configuration with a magnification of one.

# 5.2 Using the One-Dimensional Knife-Edge Method to Characterize the EUV Beam

The data collection method remains the same as described in Sec. 2, with only a few parameters changed. The beam is measured at 36 different positions along the optical axis, with a step size of  $0.5\,\mathrm{mm}$ . The transverse step size is  $5\,\mu\mathrm{m}$ , and intensity measurements are taken at 50 positions. A reflective mirror is used to direct the beam into a PCO-EUV camera for intensity measurements.

The noise in the gathered data is considerably higher than in Sec. 2, which can be attributed to the generation via HHG, which is governed by a probabilistic process [10]. This increased noise aggravates data analysis: It is no longer effective to calculate the numerical derivative and then fit a Gaussian function to extract the beam width. Excessive smoothing would be required to be able to fit a Gaussian. However, fitting an error function (erf) to the gathered data works well, and this fit will be used directly to extract the beam width. This is equivalent to taking the derivative of the fitted error function and then calculating the beam width from the resulting Gaussian:

$$P(x) = c \cdot \left(1 - \operatorname{erf}\left(\frac{\sqrt{2}(x - x_0)}{w}\right)\right) + d \stackrel{!}{=} a \cdot \operatorname{erf}\left(b \cdot (x - d)\right) + \tilde{c}$$

$$\Rightarrow b = \frac{\sqrt{2}}{w} \Rightarrow w = \frac{\sqrt{2}}{b}$$
(5.2)

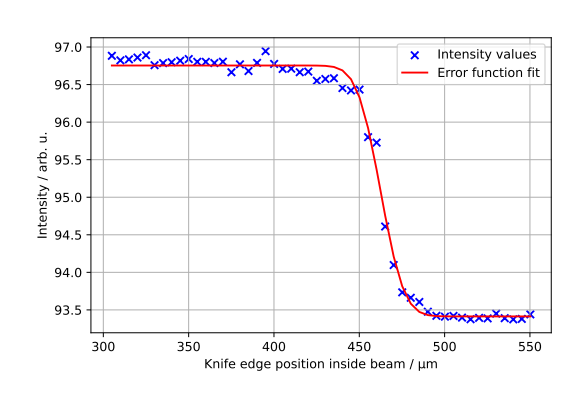
#### 5.3 Results

The fitted error functions can be seen in Fig. 5.1b. For better visibility, we do not include the data points in this plot. However, an exemplary fit with the data points is shown in Fig. 5.1a. From these error functions, the beam waists w were extracted according to eq. 5.2. The error functions already indicate that there is no significant change in the beam radius over a relatively large range along the optical axis, as the maximum slope appears to remain more or less constant. Plotting the beam waists supports this observation. We fit a linear regression to the beam waist since the waist is only varying slowly. The linear fit illustrates whether there is a visible trend for the waist along the

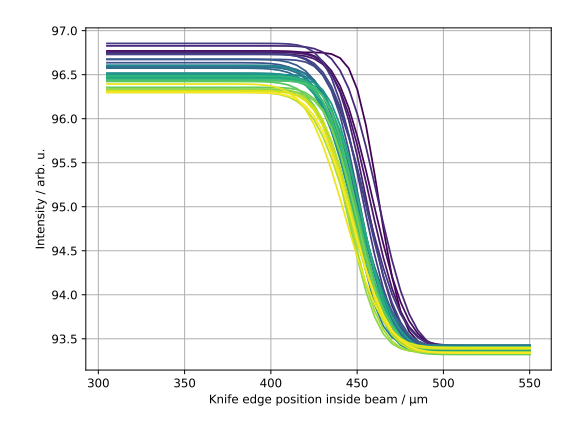
optical axis. This linear trend line shows a slight upward slope, but this can be attributed to the outlier at the first position. Since the toroidal mirror only weakly focuses the beam, it is not surprising that the focal plane cannot be pinpointed more precisely. Using eq. 1.3 we can estimate the Rayleigh range:

$$z_R = \frac{\pi w_0^2}{\lambda} = \frac{\pi \cdot 31^2 \ \mu \text{m}}{0.05 \ \mu \text{m}} \approx 60 \ \text{mm}$$
 (5.3)

Thus, the beam waist remains nearly constant over this distance along the optical axis.



(a) Knife-edge data for one of the positions along the optical axis. An error function got fitted to the data.



(b) Fitted error functions to the knifeedge data of the EUV beam, focused by the toroidal mirror. The data points were omitted for visibility. The colors represent the position along the optical axis, ranging from light to dark.

Figure 5.1: Error function fits for the EUV beam.

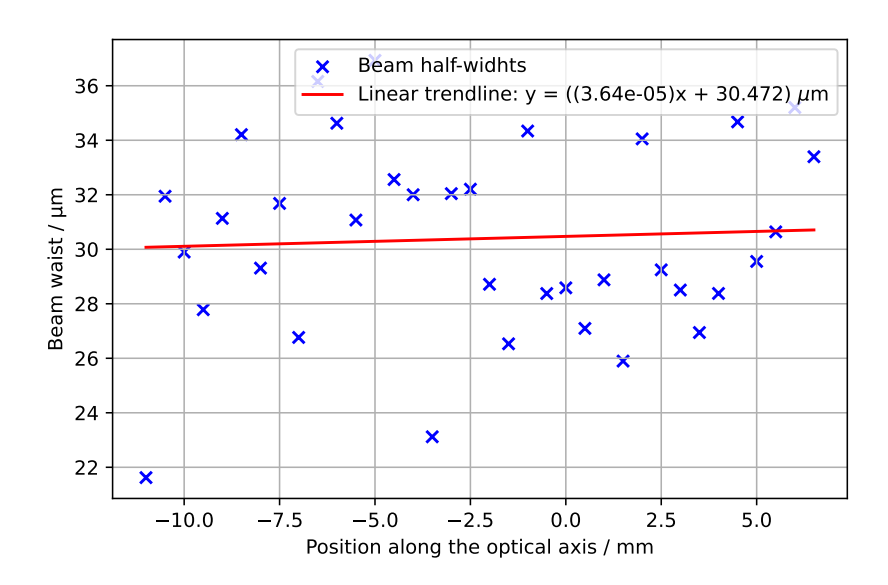


Figure 5.2: Measured beam waists along the optical axis including a linear trendline. A toroidal mirror is used to focus the beam.

We plan to use a photodiode in the future to measure the intensity when the beam passes through a metasurface with very short focal length of around 1 mm. In this case,

the beam waist increases rapidly after the focal plane. The camera then can not be brought close enough to gather all of the outgoing beam since in our setup its attached to the outside of the vacuum chamber. A photodiode could catch most of the outgoing light since it can be placed inside the vacuum chamber and close to the focal plane. This eliminates the need for imaging optics to project the beam onto a camera sensor.

## 6 Conclusion

The one-dimensional knife-edge measurement provided reasonable results. As shown in Fig. 2.6, it makes sense that the result from the knife-edge method yielded a slightly smaller value  $(w_{0,knife} = (7.6 \pm 1.4) \, \mu\text{m})$  compared to the result from the camera sensor directly  $(w_{0,img,vertical} = (8.7 \pm 0.7) \, \mu\text{m})$ . Furthermore, the figure also suggests that we are not working with an ideal Gaussian beam, as the fit deviates near the focus. A different function for the beam waist may be able to provide a better fit to our data.

Probably the most interesting result of this thesis is the implementation of the two-dimensional method. This method allows for pixel-like measurement of the beam profile and offers major advantages over the one-dimensional method: First, the two-dimensional profile of the beam can be measured, similar to a camera sensor. However, we are no longer limited to wavelengths for which high-resolution sensors exist. Second, unlike the one-dimensional method, we do not need to make assumptions about the beam's shape to obtain information about its total profile. However, the two-dimensional method has one major disadvantage: Increasing transverse resolution results in a quadratic increase in data points and therefore measurement time. A possible solution might be to combine the two methods — first using the one-dimensional method to locate the focal plane along the optical axis, and then producing a single two-dimensional profile at this focal position. Another disadvantage of the two-dimensional method is its lower signal to noise ratio compared to the one-dimensional method. As already explained earlier, this comes from the fact, that the one-dimensional method effectively integrates over one dimension, which reduces noise.

Simulations already suggest that the developed methods could be applied to higherorder modes and more complex beams. For such cases, both the one- and two-dimensional methods could be useful. For noisy signals, the one-dimensional technique should yield a higher signal to noise ratio, allowing small bumps in the intensity distribution to remain visible, which might be undetectable with the two-dimensional method. However, the two-dimensional method has the advantage when one wants to characterize the overall shape of the beam profile.

The adaptation of the developed measurement protocol for the EUV beamline was successful in measuring the focus produced by a toroidal mirror. However, a camera was used to measure the intensity. For the future application of characterizing the focus produced by metasurfaces, the camera will need to be replaced by a photodiode.

Furthermore, it will be interesting to explore the limits of the developed methods. As seen in Fig. 5.1a, measured values begin to deviate strongly from the fit function when characterizing an EUV beam focused by a toroidal mirror. We expect this effect to be more pronounced in two-dimensional measurements, as their signal to noise ratio is lower according to our simulations. Conducting multiple measurements at the same position might help smooth the data. For such measurements, we could also calculate a meaningful error for each data point by using the standard deviation of the measurements.

## References

- [1] M. Ossiander et al. "Extreme ultraviolet metalens by vacuum guiding". English. In: Science 380.6640 (2023), pp. 59–63. DOI: 10.1126/science.adg6881.
- [2] L. Novotny and B. Hecht. *Principles of Nano-Optics*. Cambridge: Cambridge University Press, 2012. ISBN: 9780511794193.
- [3] W. Plass et al. "High-resolution knife-edge laser beam profiling". In: Optics Communications 134.1 (1997), pp. 21–24. DOI: https://doi.org/10.1016/S0030-4018(96)00527-5.
- [4] A. E. Siegman. *Lasers*. Mill Valley: University Science Books, 1986. ISBN: 0-935702-11-5.
- [5] M. A. De Araújo et al. "Measurement of Gaussian laser beam radius using the knife-edge technique: improvement on data analysis". In: *Applied Optics* 48.2 (Jan. 2009), pp. 393–396. DOI: 10.1364/ao.48.000393.
- [6] J. M. Khosrofian and B. A. Garetz. "Measurement of a Gaussian laser beam diameter through the direct inversion of knife-edge data". In: *Appl. Opt.* 22.21 (Nov. 1983), pp. 3406–3410. DOI: 10.1364/A0.22.003406.
- [7] scipy. (Accessed on 11.01.2025). URL: https://docs.scipy.org/doc/scipy/reference/generated/scipy.optimize.curve\_fit.html#scipy.optimize.curve\_fit.
- [8] W. Demtröder. Experimentalphysik 2 Elektrizität und Optik. Berlin: Springer-Verlag, 2008. ISBN: 978-3-540-68219-6.
- [9] C. Kircher. Errorfunction for Excel. (Accessed on 27.10.2023). URL: https://github.com/chchurcher/ExcelErrorFunction.
- [10] Robert W. Boyd. *Nonlinear Optics*. 4th. Burlington: Academic Press, 2019. ISBN: 9780128110027.

## List of Figures

| 1.1 | Left panel: beam waist evolution of a focused Gaussian laser beam. The color map represents its intensity distribution. The dashed gray line indicates the Rayleigh range $z_R$ . Right panel: intensity distribution of the Gaussian beam profile in the focal plane. The blue dashed line indicates where the beam width is measured according to common convention [2].  | 5  |
|-----|---|----|
| 2.1 | Illustration of the knife-edge blocking part of the laser beam. The black bars indicate where the camera sensor sits. If the knife is placed in front of the focus, the camera will show the knife-edge at the top. If the knife is placed after the focus, the camera shows the knife-edge at the bottom. The two panels on the right show what the camera would capture when the knife is positioned in front of or behind the focal plane, respectively.   | 6  |
| 2.2 | Illustration of the functions that describe the experiment. $z_0$ is the position of the focal plane along the optical axis. The error functions on the left describes the drop-off in transmitted Power $P(x)$ that happens when the knife-edge is moved into the beam. The right graphs show the derivatives of the left ones. They resemble the Gaussian intensity distribution of the beam. The red graphs are at the focal plane $z_0$ and the blue graphs are $\Delta z$ away from the focal plane. The knife-edge is indicated as the gray area, which cuts of the Gaussian intensity distribution | 8  |
| 2.3 | Illustration of the experimental setup. A 520-nm wavelength laser is focused by lens L1. The knife-edge is placed on nano-stages, that can move the knife perpendicular and parallel to the beam. A beam splitter and an ND filter are used to reduce the intensity hitting the CMOS camera   | 8  |
| 2.4 | 12 selected images from the camera, processed for better visibility. These images are cropped to show only the beam. They demonstrate how the knife moves through the beam when it is close to the focus  | 9  |
| 2.5 | Experimental data and its numerical derivative. The experimental data is plotted on the left side (blue) and fitted with an error function (red). The numerical derivative of the data points (blue) can be seen on the right side. It is calculated via the finite difference method and then fitted with a Gaussian (orange). The position changes by $50\mu\mathrm{m}$ along the optical axis for every row of graphs. The errors of the fitted parameters were calculated according to eq.2.2   | 10 |
| 2.6 | Fitted data for the beam waist $w(z)$ . The fit function is given by eq. 1.3. The data points are marked in red. The minimum of the fit is marked in green  | 11 |
| 2.7 | CMOS image used to determine the beam waist in the focal plane  | 13 |
| 2.8 | Camera data along the vertical (left panel) and horizontal (right panel) direction. The remaining dimension was summed  | 13 |
| 2.9 | Vertical (left panel) and horizontal (right panel) cross sections through the center of the beam  | 14 |
| 3.1 | Image by the CMOS camera of the beam while the L-shaped knife moves through it  | 15 |

| 3.2 | Experimentally determined intensity distributions. The upper two images         |    |
|-----|---|----|
|     | are about 1 and 0.5 mm before the focus. The intensity is scaled from 0 to      |    |
|     | 1. Intensity of 1 corresponds to the maximum in the bottom-left image,          |    |
|     | which is closest to the focal plane. The bottom right image is about 0.5 mm     |    |
|     | after the focus.  | 16 |
| 4.1 | The left column of images shows the beam profiles from the simulation of        |    |
|     | the $I_{LG}(\rho, l=2, p=0)$ -mode. The images in the right column show the     |    |
|     | results of the simulated knife-edge measurements with added noise level of      |    |
|     | 0.15. The "x" markers indicate the positions of the knife. The graphs in        |    |
|     | the second and third row show the same data as in the first row, however        |    |
|     | summed along one axis. They correspond to one-dimensional beam profiles.        | 19 |
| 4.2 | The left column of images shows the beam profiles from the simulation of        |    |
|     | the $I_{LG}(\rho, l = 0, p = 2)$ -mode. The images in the right column show the |    |
|     | results of the simulated knife-edge measurements with added noise level of      |    |
|     | 0.08. The "x" markers indicate the positions of the knife. The graphs in        |    |
|     | the second and third row show the same data as in the first row, however        |    |
|     | summed along one axis. They correspond to one-dimensional beam profiles.        | 20 |
| 5.1 | Error function fits for the EUV beam  | 22 |
| 5.2 | Measured beam waists along the optical axis including a linear trendline.       |    |
|     | A toroidal mirror is used to focus the beam                                     | 22 |

## A Measurement Software

In this section, we discuss the software we used and how it was employed, particularly with regard to the movement of the attoCUBE nano-positioners and data acquisition through the CMOS camera sensor.

For roughly adjusting the position of the stages before starting actual measurements, the *attoDISCOVERY* interface that comes with the controller of the nano-positioners was helpful. This interface allows for adjusting the stages to a specific relative or absolute position by simply typing in a desired distance or position. The movement of the knife-edge can be monitored via the CMOS camera, provided the laser is running. The camera was operated through an existing Python script from the laboratory group. This setup allowed for finding a rough starting position for the knife-edge measurements. However, since we needed to acquire many data points at different positions inside and along the beam, it made sense to write Python scripts to automate the process.

Using the Python package provided by *attoCUBE*, called *AMC-API*, two functions were implemented to move the stage in either an absolute or relative manner. The distance or end position, along with the stage to be moved, could be specified as input parameters.

With this setup, we were able to write functions that automatically conduct the measurements by using the move functions and an adapted version of the camera script. The only necessary input parameters for this data-gathering function are the start position, the number of steps along the different axes, and the corresponding step size. The function for the two-dimensional method works in the same manner, just with two more input parameters, since a third stage also has to be operated.

While the data was being gathered, the camera image could be monitored, and the total intensity value as well as the absolute position were stored after every stage movement (refer to 2.2). For the one-dimensional measurement, the fitting routine and data evaluation were not very resource-intensive, so it made sense to directly include them in the script, allowing the change in beam diameter to be observed as the knife was moved to a new position along the optical axis. For the two-dimensional knife-edge measurement, the data evaluation was performed separately at a later stage.

We later adapted the code to work with the EUV camera, so it could be used to measure the focus of the toroidal mirror.